

UCRL-97250
PREPRINT

"MODERATE-m" BALLOONING MODES
in
QUADRAPOLE STABILIZED TANDEM MIRRORS

W.M. Nevins
L.D. Pearlstein

CIRCULATION COPY
SUBJECT TO RECALL
IN TWO WEEKS

This paper was prepared for submittal to
PHYSICS OF FLUIDS

August 4, 1987

Lawrence
Livermore
National
Laboratory

This is a preprint of a paper intended for publication in a journal or proceedings. Since changes may be made before publication, this preprint is made available with the understanding that it will not be cited or reproduced without the permission of the author.

DISCLAIMER

This document was prepared as an account of work sponsored by an agency of the United States Government. Neither the United States Government nor the University of California nor any of their employees, makes any warranty, express or implied, or assumes any legal liability or responsibility for the accuracy, completeness, or usefulness of any information, apparatus, product, or process disclosed, or represents that its use would not infringe privately owned rights. Reference herein to any specific commercial products, process, or service by trade name, trademark, manufacturer, or otherwise, does not necessarily constitute or imply its endorsement, recommendation, or favoring by the United States Government or the University of California. The views and opinions of authors expressed herein do not necessarily state or reflect those of the United States Government or the University of California, and shall not be used for advertising or product endorsement purposes.

"MODERATE- m " BALLOONING MODES
in
QUADRAPOLE STABILIZED TANDEM MIRRORS*

W.M. Nevins and L.D. Pearlstein
Lawrence Livermore National Laboratory
Livermore, Ca 94550 USA

ABSTRACT

The β -limits on the central cells of non-axisymmetric tandem mirrors due to moderate- m ballooning modes are studied. Both finite-Larmor-radius effects and corrections associated with the finite extent of the ballooning modes in the plane perpendicular to \mathbf{B} are retained. The assumption of short perpendicular wavelength together with the large ellipticity of the flux surfaces near the magneto-hydrodynamic (MHD) anchor cells allows a reduction of the three dimensional problem into a sequence of three one-dimensional problems. The marginal stable boundary for the Mirror Fusion Test Facility (MFTF-B) is calculated, and compared with that obtained from a low mode number calculation.

* This work was performed under the auspices of the U.S. Department of Energy by the Lawrence Livermore National Laboratory under contract number W-7405-ENG-48.

1. INTRODUCTION

Ballooning modes have been studied extensively in connection with magnetic confinement of plasmas because these modes should limit the plasma pressure that can be contained by a given magnetic field. The figure of merit is $\beta = 8\pi P/B^2$, where P is the plasma pressure and B is the magnitude of the magnetic field. In the past few years a great deal of progress has been made in analyzing ballooning modes by employing the "large- m " expansion,¹ which allows one to reduce the ideal MHD ballooning mode problem to the solution of a second order ordinary differential equation along each magnetic field line. More recent analyses in axisymmetric systems (e.g., tokamaks) have demonstrated that modifications associated with the radial mode structure (the " $1/m$ corrections")² and with kinetic effects³ (charge separation due to the difference between the electron and ion gyroradius, FLR effects⁴) improve the stability boundaries.

In this paper we present an analysis of the limit on β due to ballooning modes in quadrupole stabilized tandem mirrors, including both effects. We will focus on the tandem mirror configuration MFTF-B at the Lawrence Livermore National Laboratory.^{5,6} We find that these corrections have such a strong stabilizing effect that the beta limits are not set by ideal MHD ballooning modes in this machine. In fact, we believe that these stabilizing terms are so important that it is unlikely that these modes will set the beta limits in any current or future quadrupole stabilized tandem mirror experiments.

An analysis of ballooning modes in non-axisymmetric systems which includes both corrections requires the solution of a three dimensional eigenvalue problem. We accomplish this by utilizing a separation in time scales to reduce the three dimensional problem to a sequence of three quasi-one-dimensional problems. Ballooning modes are essentially shear Alfvén waves. Hence, the most rapid communication time is along the magnetic field. It is this rapid communication that allows one to decouple the variation in the ballooning mode eigenfunction along the magnetic field from the variations across \mathbf{B} , and thereby obtain to this order an ordinary differential equation along the magnetic field.¹⁻³

In axisymmetric systems there is only one remaining non-ignorable coordinate, so the resolution of the radial mode structure becomes a relatively straight-forward one dimensional problem.^{2,7} Using the WKB approximation only one constant of the ray motion, the frequency of the ballooning mode, is required to guarantee the integrability of the ray equations of motion. However, in non-axisymmetric systems we are left with a two-dimensional problem in the plane perpendicular to \mathbf{B} . We are able to solve this two dimensional problem by using the formalism of semi-classical mechanics (essentially WKB theory extended to several dimensions).⁸ An analysis of ray trajectories shows that there is an additional separation in time scales associated with the bending of the highly elliptical flux bundles in the transition region between the MHD anchor and the center cell of a tandem mirror. This further separation in time scales allows us to reduce the remaining two dimensional problem into a sequence of two one dimensional problems. The first of these is solved by using phase integral techniques. The remaining time scale is then dealt with in the local approximation since the WKB frequency splitting associated with this long time scale is insignificant.

The plan of the paper is as follows. In Section 2 we review the “large- m ” formalism as it applies to tandem mirrors.⁹ In Section 3 we review the ideal MHD beta limits due to these ballooning modes and describe the very important structure of the concomitant eigenmodes and eigenspectra. In Section 4 we show how the formalism of semi-classical mechanics may be used to obtain a global dispersion relation which includes both kinetic effects^{2,3} and the “ $1/m$ ” corrections.² In Section 5 we describe our procedure for computing marginal stability boundaries. In Section 6 we present an analytic computation of the marginal stability boundary that is valid near ideal MHD marginal stability. In Section 7 we present numerical results for the axicell configuration of MFTF-B, and finally in Section 8 we summarize our results.

2. LARGE- m THEORY AND OTHER APPROXIMATIONS

The “finite- m ” correction to ideal MHD ballooning modes was originally developed for tokamaks^{1,2}. The “large- m ” formalism describes modes in which the typical scale length for variation of the perturbation across the magnetic field is short in comparison to either the equilibrium scale lengths, or the scale length for variations of the perturbation parallel to \mathbf{B} . An eikonal approximation, $\phi \sim \tilde{\phi}(s) \exp[iS(\theta, \psi)]$, is then employed to describe the perpendicular variations in the stream function, ϕ , which describes the perturbation. The assumption of rapid perpendicular variation allows one to reduce the MHD ballooning mode problem to the solution of a second order ordinary differential equation along each magnetic field line.¹⁻³

The equation is most simply written in magnetic flux coordinates, (s, θ, ψ) , where ψ , the enclosed magnetic flux, labels a particular flux surface; θ is an angle-like variable that labels a particular magnetic field line on this flux surface; and s measures the position along this magnetic field line. In the work reported here we use the long-thin, or paraxial expansion.¹⁰ To lowest significant order in the long-thin parameter, $\lambda = R/L$ (R is a typical radial dimension and L is a typical axial dimension) there is no difference between s and the axial distance, z . Hence, we may write the ballooning mode equation as a second order differential equation in z :

$$\left[\frac{d}{dz} \frac{Q |\nabla S|^2}{B^3} \frac{d}{dz} + \frac{\rho(z)}{B^3} |\nabla S|^2 (\omega^2 - \omega S_\theta \Omega_{*i}) - \frac{1}{B^3} (\hat{\mathbf{b}} \times \nabla (P_\perp + P_\parallel)) (\mathbf{K} \times \hat{\mathbf{b}}) : \nabla S \nabla S \right] \tilde{\phi} = 0 \quad (1)$$

where $Q = B^2 + P_\perp - P_\parallel$ is the parallel component of the total stress tensor,¹⁰ B is the magnetic field strength, $\rho(z)$ is the mass density, ω is the wave frequency, $S_\theta \equiv \partial S / \partial \theta$ is proportional to the surface component of the wave vector. Here $\Omega_{*i} = -(B / \rho \omega_{ci}) (\partial P_\perp / \partial \psi)$, where ω_{ci} is the ion cyclotron frequency, so that $S_\theta \Omega_{*i}$ is the standard diamagnetic drift frequency. P_\perp and P_\parallel are the perpendicular and parallel pressures, $\mathbf{K} = \hat{\mathbf{b}} \cdot \nabla \hat{\mathbf{b}}$ is the magnetic curvature, and $\hat{\mathbf{b}}$ is a unit vector parallel to the magnetic field. In this work we have ignored the finite β corrections to the FLR term (see Ref. 3). This approximation

is justified because we find that Eq. (1) properly describes the most unstable modes only at modest values of the center cell beta, $\beta_c \leq 0.1$, where the low β FLR term dominates. Because of its length the central cell produces the dominant FLR term.

We will solve this equation subject to the boundary condition $\partial\bar{\phi}/\partial z = 0$ at the axial boundaries of the plasma; this is a free, or insulating boundary condition (as opposed to a conducting, or “line-tied” boundary condition). This boundary condition follows from requiring that the perturbed current vanish in the vacuum external to the plasma. As a consequence the structure of the magnetic field beyond the lateral boundaries of the plasma is left unaltered by the perturbation, although the labels of magnetic field lines in the vacuum may be interchanged. It is necessary to find MHD equilibria in order to evaluate the coefficients in Eq. (1). Non-axisymmetric tandem mirror equilibria are obtained by using the expansion described in Ref. 11. This involves expanding in both the long-thin parameter, λ , and in $\beta = 8\pi P/B^2$.

A final approximation in the present work is to treat Ω_{*i} as constant, independent of θ, ψ , and z . This approximation can be relaxed with a considerable increase in numerical computation time. If Ω_{*i} varies slowly in the region over which the modes are localized, as is generally the case, this “local limit” is reasonable. Moreover this FLR term is most important in the long center cell of tandem mirror,¹² where Ω_{*i} is nearly constant. We will see in Sec. 5 how this approximation greatly simplifies the system of equations that must be solved numerically to obtain the marginal stability boundary for ballooning modes in a given magnetic configuration.

3. IDEAL MHD RESULTS

Previous analysis of beta limits in quadrupole stabilized tandem mirrors¹³ have been based on a study of ideal MHD ballooning modes in the “large- m ” limit. We review the principle results of these ideal MHD ballooning mode calculations here because they will provide a basis for understanding the full three-dimensional treatment, including both the kinetic term and the “ $1/m$ ” corrections described in the next section. The ideal MHD ballooning mode equation may be obtained from Eq. (1) by taking the limit $\Omega_{*i} \rightarrow 0$. Since Ω_{*i} is proportional to a_i/R , this is equivalent to considering a very large diameter machine, in which the ion gyroradius, a_i , is very much less than a radial scale length, R . In the ideal MHD limit each term in the ballooning mode equation is proportional to $|\nabla S|^2$. Dividing the equation through by its value at the midplane of the center cell, we obtain an equation which depends only on the orientation of ∇S . In the ideal MHD limit Eq. (1) provides no information about the magnitude of ∇S .

This orientation may be represented by

$$\Gamma \equiv 2\psi S_\psi / S_\theta \quad (2)$$

The angle, Υ , between ∇S and the flux surface at the midplane of the center cell (see Fig. 1) is given by

$$\Upsilon = \arctan \Gamma. \quad (3)$$

It is found that the marginal stability condition for ideal MHD ballooning modes in non-axisymmetric tandem mirrors depends on both the field line labels (θ, ψ) and on Γ . At small to moderate values of β_p , the “worst” field line (i.e., the last field line on which ideal MHD ballooning modes are unstable as β_c is decreased) always occurs at $\theta = 0, \pi/2$. These field lines lie on one of the principle axes of the elliptical flux surfaces. Due to the standard symmetry of quadrupole tandem mirrors we need only consider one quadrant. Hence, we need only consider MHD stability in the neighborhood of $\theta = 0$. In this and all that follows the subscript “a” refers to the quadrupole MHD anchor cell, the subscript “p” refers to the axisymmetric electrostatic plugging cell, and the subscript “c” refers to the central cell

The worst value of ψ generally lies about midway out in the radial profile. Figure 2 shows the critical value of β_c for marginal stability in MFTF-B vs. ψ . The peak value of β in the MHD anchor cell is held fixed at $\beta_a = .55$, while θ and Γ have been chosen to minimize β_c . Negative values of β_c appear in Fig. 2 because stability to ideal MHD infinite- m ballooning modes was not a design requirement for MFTF-B. It was recognized, as a result of the calculations described here, that the kinetic effects would stabilize the infinite- m ballooning modes. Mathematically, we have obtained marginal stability boundaries by artificially allowing negative pressures, and hence, negative β in the center cell. We see that the worst flux surface at $\psi/\psi_{edge} = 0.48$ lies at the bottom of quite a gentle well in critical β_c . Similarly, in Fig. 3 we show the critical value of β_c vs. Γ for the same values of β_a and β_c . In Fig. 3 θ is held fixed at zero and ψ is fixed at $\psi/\psi_{edge} = 0.48$, the worst field line for $\Gamma = 0$. We see that the worst orientation, $\Gamma = 0$, lies at the bottom of a very steep well in Γ . When Γ varies from 0 to .25, the critical value β_c increases by 15%.

The most striking feature of these results is the strong dependence of the center-cell beta limit on the orientation of ∇S . Mathematically, this strong dependence results from the field line bending term in Eq. (1),

$$\frac{d}{dz} \frac{Q|\nabla S|^2}{B^3} \frac{d}{dz} \tilde{\phi}.$$

The z -dependence of the coefficient in this term is dominated by the variation of $|\nabla S|$ with z . Although S is independent of z ,

$$\nabla S = S_\psi \nabla \psi + S_\theta \nabla \theta \quad (4)$$

has a strong z -dependence because of the z -dependence of the covariant basis vectors, $\nabla \psi$ and $\nabla \theta$. This dependence, which is purely a result of the equilibrium flux surface geometry, is most pronounced in the neighborhood of the transition regions where the flux surfaces are highly elliptical. We may gain some insight into the behavior of this term by temporarily ignoring the finite-beta corrections to the vacuum flux surfaces. The flux surface geometry may then be obtained analytically.¹³ The basis vectors satisfy

$$|\nabla \psi|^2 = 2\psi \left[\frac{\cos^2 \theta}{\sigma^2(z)} + \frac{\sin^2 \theta}{\tau^2(z)} \right], \quad (5)$$

$$|\nabla\theta|^2 = \frac{1}{2\psi} \left[\frac{\sin^2 \theta}{\sigma^2(z)} + \frac{\cos^2 \theta}{\tau^2(z)} \right], \quad (6)$$

and

$$\nabla\theta \cdot \nabla\psi = - \left[\frac{1}{\sigma^2(z)} - \frac{1}{\tau^2(z)} \right] \sin \theta \cos \theta; \quad (7)$$

where

$$x = \sqrt{2\psi}\sigma(z) \cos \theta, \quad (8)$$

and

$$y = \sqrt{2\psi}\tau(z) \sin \theta, \quad (9)$$

are the coordinates of a field line, while $B_v(z) = 1/\sigma(z)\tau(z)$ is the magnitude of the vacuum magnetic field. The partial derivatives of S may be written in terms of Υ as

$$S_\psi = \frac{S_0}{2\psi} \sin \Upsilon \quad (10)$$

and

$$S_\theta = S_0 \cos \Upsilon. \quad (11)$$

Hence, $|\nabla S|^2$ varies with ψ, θ, Υ , and z as

$$|\nabla S|^2 = \frac{S_0^2 B_v}{2\psi} \left[\frac{\sin^2(\Upsilon - \theta)}{\sigma^2(z)} + \frac{\cos^2(\Upsilon - \theta)}{\tau^2(z)} \right]. \quad (12)$$

If the major axis of the elliptical flux surface is nearly vertical ie $\tau \gg \sigma$ in the region where field line bending occurs, then the bending energy is minimized when $\sin(\Upsilon - \theta) \simeq 0$. Small departures of $(\Upsilon - \theta)$ from zero introduce a large term, proportional to τ^2/σ^2 , into the bending energy. Note that the bending energy is minimized when ∇S is nearly parallel to the major axis of the elliptical flux surface. Flux bundles are bent in the direction $\xi \sim \nabla S \times \mathbf{B}$. Hence, the perturbations that minimize the bending energy are those that bend flux bundles perpendicular to the flat plane of the elliptical flux surfaces. This observation motivates an analogy between these elliptical flux bundles and a flat steel spring. Such a spring is easily bent in the plane perpendicular to its flat surface; but it is very difficult to bend within the flat plane. The normal modes of such a system have two distinct time scales; a high frequency associated with perturbations that bend the spring (or flux bundle) in its flat plane, and a low frequency associated with perturbations which bend the spring perpendicular to this plane. In Sec. 4 we will show that the propagation of ballooning modes in quadrupole stabilized tandem mirrors exhibits these two disparate time scales. It is this separation of time scales that allows us to reduce the two dimensional problem across \mathbf{B} into a sequence of two quasi-one-dimensional problems.

We will show in Sec. 7 that the ideal MHD results presented in this section are far too pessimistic. When effects associated with the perpendicular structure (i.e., “1/m

corrections”) and charge separation due to finite ion gyroradius (i.e., “kinetic terms”) are included the beta limit is greatly increased. For the example considered here, MFTF-B, ideal infinite- m calculations yield instability even at $\beta_c = 0$ as there is enough pressure in the axisymmetric plug cell (which has bad curvature) to drive ballooning modes. The finite- m calculations described below yield a the central cell beta limit somewhere in the range $.1 < \beta_c < .22$. This result is in part due to the stabilizing kinetic term, which acts over the entire axial length of the tandem mirror, while the destabilizing pressure-curvature term acts only in the axicell and the transition region between the axicell and the MHD anchor cell; and in part due to the “ $1/m$ corrections”. The latter improvement is due to the fact that the orientation of the perpendicular wave vector, as described by Γ , is determined by the perpendicular structure of the mode, and is no longer free to be adjusted so that it fits into the deep well in Fig. 3 near $\Gamma = 0$.

4. METHOD OF SOLUTION

The stabilizing kinetic effects enter Eq. (1) through a term proportional to S_θ . Unfortunately, the single field line problem provides no information about the magnitude of this term; this information must be obtained from a solution of the eigenvalue problem in the plane perpendicular to \mathbf{B} . We find that it is necessary to include the kinetic term when analyzing the perpendicular mode structure because this problem becomes singular in the limit $\Omega_{*i} \rightarrow 0$ (see Sec. 6). This is in contrast to the ballooning mode problem in axisymmetric systems, like tokamaks, where S_θ is a constant of the ray motion so that the kinetic term and the radial mode structure (which leads to the “ $1/m$ corrections”)² can be analyzed independently. In non-axisymmetric systems, like quadrupole stabilized tandem mirrors, these two problems are coupled through S_θ , so that they must be treated together.

Equation (1) describes the behavior of “large- m ” (i.e., $S_\theta \gg 1$) ballooning modes on each magnetic field line. A numerical solution of this equation along a particular field line yields the local dispersion relation,

$$D(\theta, \psi, \Gamma, \Omega^2; \beta_c, \beta_a \dots) = 0. \quad (13)$$

The explicit dependence on S_θ enters through the parameter

$$\Omega^2 = \omega(\omega - S_\theta \Omega_{*i}). \quad (14)$$

Note that the local dispersion relation depends not only on the field line labels (θ, ψ) and the wave parameters ∇S and ω ; but also on the equilibrium parameters Ω_{*i}, β_c , etc. Our problem is to “sew” the solutions on each field line together in a self-consistent way to obtain both the mode structure in the (θ, ψ) plane and the global dispersion relation. We accomplish this by using the theory of semi-classical mechanics—essentially WKB theory generalized to many dimensions. In the semi-classical formalism the local dispersion relation D may be viewed as the Hamiltonian governing the motion of a ray in the four dimensional phase space, $(\theta, \psi, S_\theta, S_\psi)$, where the field line labels (θ, ψ) are the coordinates, and the covariant components of ∇S , (S_θ, S_ψ) , are the conjugate momenta.

The ballooning mode ray then obeys the equations of motion

$$\dot{\theta} = \frac{\partial D}{\partial S_\theta}, \quad (15)$$

$$\dot{\psi} = \frac{\partial D}{\partial S_\psi}, \quad (16)$$

$$\dot{S}_\theta = - \frac{\partial D}{\partial \theta}, \quad (17)$$

and

$$\dot{S}_\psi = - \frac{\partial D}{\partial \psi}. \quad (18)$$

The ray motion described by Eqs. (15)–(18) may be either integrable or stochastic.¹⁴ The Hamiltonian D is clearly a constant of the ray motion since the ray must stay on the surface $D = 0$. If there is a second independent constant of the motion, then the ray orbit must lie on a two dimensional surface, Σ , embedded in the four dimensional phase space. It can be shown that the surface Σ is topologically a torus. This surface is central to the semi-classical theory of mechanics, where it is known as the “invariant torus”. Ray orbits that lie on an invariant torus are said to be integrable. If a second constant of motion does not exist, then the ray orbit fills a three dimensional region of phase space (the energy shell), and the ray orbit is said to be stochastic.

The theory of semi-classical mechanics is concerned primarily with integrable systems. If the ray orbits are stochastic little can be said about the mode spectrum; while if the ray orbit is integrable, then the dispersion relation may be obtained by quantizing the two independent actions,

$$I_k = \oint_{C_k} dq \cdot \nabla S. \quad (19)$$

These two independent actions are obtained by following a closed path that goes either once around the invariant torus the short way (C_1), or else once around the torus the long way (C_2). This is illustrated in Fig. 4. The quantization condition for the systems considered here is

$$I_k = (2n_k + 1) \pi. \quad (20)$$

We find that the modes associated with the larger values of n_k are more stable than the $n_k = 0$ modes. Hence, in studying marginal stability one need only consider normal modes satisfying

$$I_k = \pi. \quad (21)$$

Before attempting to apply the methods of semi-classical mechanics we must determine if the ray orbits associated with “large- m ” ballooning modes in the axicell configuration of MFTF-B are integrable. This is accomplished by a direct numerical integration of the ray equations of motion. A ray is initialized with a particular set of phase variables $(\theta_0, \psi_0, S_{\theta 0})$. The fourth phase variable, $S_{\psi 0}$, is chosen such that the ray lies on the

“energy shell”, $D = 0$. The orbit is advanced in time using Eqs. (15)–(18) together with the Livermore Solver for Ordinary Differential equations (LSODE)¹⁵. At each time step the ballooning mode equation, (1), is integrated on the current field line to calculate D and its derivatives. The value of D is monitored to check the accuracy of the integration. Integrability may then be determined from a Poincaré map;¹⁶ Each time that the ray passes through the hyper-plane $\psi = \psi_0$, the current values of θ and S_θ are plotted. If the ray orbit is integrable, then these points will lie on a smooth curve as in Fig. 5, while if the ray orbit is stochastic then they will fill an area in the (θ, S_θ) plane. Figure 6 shows a stochastic orbit. We did not follow this orbit long enough to see this area-filling property in the Poincaré map.

We find that the ray orbits are often, but not always integrable. When the equilibrium parameters are in the general vicinity of ideal MHD marginal stability the ray orbits are found to be integrable; while as we move further from ideal MHD marginal stability (by increasing β_c , for example), this integrability breaks down. This loss of integrability occurs because far from ideal marginal stability the field line bending term can be balanced by the kinetic and inertial terms in the center cell. Hence, the axial eigenfunctions that we obtain in this regime show substantial field line bending occurs in the center cell where the flux bundles are nearly circular, in addition to bending in the transition region between the axisymmetric plug cell and the MHD anchor cell where the flux bundles are strongly elliptical. As a result, the time scale separation is lost far from ideal marginal stability. The assumption that $S_\theta \gg 1$ also breaks down for the most unstable modes far from ideal MHD marginal stability, so that this loss of integrability does not by itself limit our calculation.

It is really somewhat remarkable that the any ray orbits are found to be integrable, as it is an unfortunate fact of classical mechanics that most two dimensional Hamiltonian systems are not integrable. There are two general cases in which two dimensional systems become integrable. Either there is a symmetry (perhaps a hidden one), or there is a separation of time scales. Our system is an example of one in which there is a separation in characteristic time scales of the ray motion. This may be seen in the projection of the ray orbit into the (θ, ψ) plane shown in Fig. 5. There is a rapid motion directed generally parallel to $\nabla\psi$ superimposed on a slow precession in θ . This separation of time scales is associated with the extreme ellipticity of the equilibrium flux surfaces in the transition regions. Ballooning modes are associated with the bending of flux bundles in this transition region. When a flux bundle with a circular cross-section in the central cell is mapped into this region it also takes on an elliptical cross-section. As we pointed out in Sec. 3, these elliptical flux bundles act much like flat steel springs; they are easily bent perpendicular to the flat plane, but are very stiff when bent in the flat plane. Hence, the ballooning ray has a rapid quiver associated with bending the elliptical flux bundles parallel to their major axis in the transition region. The action associated with this rapid motion, I_{fast} , is then an adiabatic invariant over the slow motion. Hence, I_{fast} is the second independent constant of motion which guarantees the integrability of ray orbits.

A numerical approximation to I_{fast} may be obtained by following the ray orbit once

around the torus the short way, accumulating $\int \nabla S \cdot d\mathbf{q}$ along the ray orbit, and then closing the loop by using a two-point Simpson's rule integration to step back to the initial point along a line of constant ψ . This scheme allows us to evaluate I_{fast} once for each point on the Poincaré map. The numerically determined value of $I_{fast} - \pi$ is plotted in Figs. 5–6. The initial phase variables were chosen such that $I_{fast} = \pi$ for the first loop in order that the dispersion relation, Eq. (21), be satisfied. We see from Figs. 5–6 that I_{fast} is indeed well conserved on the integrable orbit, while it is not conserved on the stochastic orbit. The variation in the numerically determined I_{fast} on the integrable orbit in Fig. 5 is mainly due to numerical errors introduced by the two point Simpson's rule integration used to close the integration contour.

The separation of time scales also provides us with some information about the frequency spectrum. The separation in frequency between modes with neighboring values of n_{fast} is $\Delta\omega \sim 2\pi/T_{fast}$, where

$$\begin{aligned} T_{fast} &= \frac{\partial}{\partial\omega} I_{fast} \\ &= \oint d\mathbf{q} \cdot \frac{\partial}{\partial\omega} \nabla S, \end{aligned} \quad (22)$$

and the integral is to be taken once around the torus the short way. Noting that $|\partial\nabla S/\partial\omega|$ may be interpreted as $1/v_{group}$, we see that T_{fast} is essentially the period of the fast motion. Similarly, the frequency separation between modes with neighboring values of n_{slow} is $\delta\omega \sim 2\pi/T_{slow}$, where

$$T_{slow} = \oint d\mathbf{q} \cdot \frac{\partial}{\partial\omega} \nabla S, \quad (23)$$

with the integral taken once around the torus the long way (T_{slow} is essentially the area enclosed by the line segments connecting the points on the Poincaré map in Fig. 5). Hence,

$$\frac{\delta\omega}{\Delta\omega} \sim \frac{T_{fast}}{T_{slow}} \ll 1 \quad (24)$$

i.e., the line spectrum must be like that shown in Fig. 7. It follows that we need only do a careful job in quantizing I_{fast} , while the remaining parameter that determines I_{slow} may be chosen to maximize instability. This will put us within $\delta\omega$ of the most unstable mode. Instability is maximized when the derivative of I_{fast} with respect to the remaining parameter vanishes. This approximation is analogous to estimating the dispersion relation in a plasma slab by using local theory at the most unstable value of the inhomogeneous coordinate. This procedure generally does reasonably well, although it misses WKB corrections (which are usually stabilizing) associated with the radial mode structure. In the present instance, we retain WKB corrections associated with the fast motion, but ignore small stabilizing corrections associated with the slow motion. This is an important practical simplification because it is now only necessary to follow a ray once around the torus the short way and compute just I_{fast} . This in turn requires on the order of 10^3 integrations of

the balloon equation, and takes several seconds of CPU time on a CRAY-1. A numerical computation of I_{slow} (which we are avoiding) would require that we follow the ray for at least one full period of the slow motion. This requires between five and ten minutes of CPU time on a CRAY-1. Hence, ignoring corrections to the mode frequency of order $\delta\omega$ as compared to corrections of order $\Delta\omega$ saves hours of computer time in computing marginal stability boundaries.

5. MARGINAL STABILITY BOUNDARIES

It is necessary to find the invariant torus associated with the unstable "large- m " ballooning modes in order to obtain the dispersion relation and the marginal stability boundary. We expect that the most unstable ballooning modes will be localized in the neighborhood of the worst field line of ideal MHD theory. Hence, we may fix θ_0 and ψ_0 as the labels of this field line. The initial value of S_θ , $S_{\theta 0}$, then selects a particular invariant torus from among those intersected by the curve

$$\begin{aligned}\theta &= \theta_0, \\ \psi &= \psi_0, \\ D(\theta, \psi, \Gamma, \Omega^2) &= 0.\end{aligned}\tag{25}$$

Given a particular set of equilibrium parameters, the frequency of the most unstable mode satisfies the equations

$$I_{fast}(\theta_0, \psi_0, S_{\theta 0}, \Omega^2; \beta_c, \dots) = \pi\tag{26}$$

and

$$\frac{\partial}{\partial S_{\theta 0}} I_{fast} = 0.\tag{27}$$

If we require this mode to be marginally stable, we must satisfy the additional equation

$$\frac{\partial}{\partial \omega} I_{fast} = 0.\tag{28}$$

In general, marginal stability boundaries are obtained by solving the three Equations, Eqs. (26)–(28), simultaneously. A further simplification is possible if we make use of the assumption that Ω_{*i} is constant together with the assumption that S_θ has only a small fractional variation along the ray orbit during one period of the rapid motion. These assumptions allow us to replace the third equation with the condition

$$\frac{\partial}{\partial \omega} \Omega^2 = 0.\tag{29}$$

which may be solved analytically using Eq. (14) to obtain,

$$\omega = \frac{1}{2} S_{\theta 0} \Omega_{*i}.\tag{30}$$

This results in a considerable simplification, as it is now only necessary to solve two equations, Eqs. (26) and (27), simultaneously with Ω^2 set equal to $-(S_{\theta 0}\Omega_{*i}/2)^2$. Our experience indicates that the simultaneous solution of Eqs. (26) and (27) provides a very good approximation to the actual marginal stability boundary obtained by solving Eqs. (26)–(28). Evidently the assumption that S_θ has only a small fractional variation over one period of the rapid motion of the ray orbit is well satisfied.

Either set of equations may be solved numerically to find the marginally stable value of Ω_{*i} for a particular set of equilibrium parameters, $\beta_c, \beta_a, \beta_p, \dots$. Then one of these parameters, say β_c , may be varied to obtain the marginal stability boundary in the (Ω_{*i}, β_c) plane.

6. NEAR THE IDEAL MHD LIMIT

When studying ballooning modes in realistic tandem mirror equilibria the coefficients in Eq. (1) are only known numerically. Hence, Eq. (1) must be numerically integrated to obtain the local dispersion relation, Eq. (13). Nevertheless, it is possible to obtain an analytic approximation to I_{fast} that is valid for systems near ideal MHD marginal stability by expanding in both the ellipticity of the flux surface in the transition region where line bending occurs ($\epsilon \equiv \sigma/\tau \ll 1$), and then making a subsidiary expansion in the localization of the unstable eigenfunction about the worst field line ($\delta \ll 1$). The local dispersion relation has a minimum at the worst field line. In the neighborhood of this field line the local dispersion relation may be written as

$$D(\theta, \psi, \Gamma, \Omega^2) \simeq \frac{1}{2} [D_{\psi\psi}\eta^2 + \bar{D}_{\theta\theta}\xi^2] + D_{\psi\Gamma}\psi(\delta\Gamma - \kappa\xi) \\ + D_{\Omega^2}\delta\Omega^2 + \bar{D}_{\psi\theta}\eta\xi + \frac{1}{2}D_{\Gamma\Gamma}(\delta\Gamma - \kappa\xi)^2 \quad (31)$$

where $\xi = \theta - \theta_0$, $\eta = \psi - \psi_0$, $\delta\Gamma = \Gamma - \Gamma_0$, $\delta\Omega^2 = \Omega^2 + \gamma_{MHD}^2$, $\bar{D}_{\psi\theta} \equiv D_{\psi\theta} + \kappa D_{\psi\Gamma}$, and $\bar{D}_{\theta\theta} \equiv D_{\theta\theta} - \kappa^2 D_{\Gamma\Gamma}$ describes the slow variation of D with θ . Here (θ_0, ψ_0) labels the worst field line, Γ_0 determines the worst orientation of ∇S on the worst field line, γ_{MHD}^2 is the ideal MHD growth rate on the worst field line, and $\kappa = -D_{\theta\Gamma}/D_{\Gamma\Gamma}$. The coefficients of the various terms in Eq. (31) are obtained by differencing the numerically determined local dispersion relation about the worst field line, as indicated. The first five terms in Eq. (31) describe the localization of the MHD drive about the worst field line, while the orientation, Γ , of ∇S enters only in the final term. The coefficient of this last term is of order ϵ^{-2} . It is large compared to the coefficients of the other terms in Eq. (31) since the bending energy is very sensitive to Γ (see Sec. 3). The large coefficient of the final term in Eq. (31) is, as previously mentioned, the direct consequence of the large restoring force associated with bending flux bundles parallel to the major axis of the elliptical flux surfaces.

Using the fact that $\epsilon \ll 1$ together with the assumption that the mode is well localized about the worst field line [$\xi^2, (\eta/\psi_0)^2, \delta\Gamma^2, \Omega^2, \gamma_{MHD}^2 \sim \delta^2 \ll 1$], it is possible to obtain an analytic expression for a second constant of the ray motion; namely the action, I_{fast} ,

associated with the rapid time scale of the ray motion. The analytic treatment begins by noting that D is a constant of the ray motion (i.e., $D = 0$ on the ray orbit). Hence, we may set $D = 0$, and solve for $\delta\Gamma = \delta\Gamma^{(0)} + \delta\Gamma^{(1)}$ order by order in the small parameter ϵ . At lowest order we find that

$$\begin{aligned}\delta\Gamma^{(0)} &= \kappa\xi \\ &\sim \delta\epsilon^0.\end{aligned}\tag{32}$$

To first order we find

$$\begin{aligned}\delta\Gamma^{(1)} &= \pm \left\{ - \left[2(D_{\Omega^2}\delta\Omega^2 + \bar{D}_{\psi\theta}\eta\xi) + D_{\psi\psi}\eta^2 + \bar{D}_{\theta\theta}\xi^2 \right] / D_{\Gamma\Gamma} \right\}^{1/2} \\ &\sim \delta\epsilon^1.\end{aligned}\tag{33}$$

Armed with this expression for $\delta\Gamma^{(1)}$, we now proceed to analyze the ray motion. At leading order the equations of motion are given by

$$\dot{\eta} = \frac{\Gamma}{S_\psi} D_{\Gamma\Gamma} \delta\Gamma^{(1)} \sim \delta\epsilon^0,\tag{34}$$

$$\dot{\xi} \simeq -\frac{\Gamma}{S_\theta} D_{\Gamma\Gamma} \delta\Gamma^{(1)} \sim \delta\epsilon^0,\tag{35}$$

$$\dot{S}_\psi \simeq -\frac{\Gamma}{\psi} D_{\Gamma\Gamma} \delta\Gamma^{(1)} \sim \delta\epsilon^{-1},\tag{36}$$

$$\dot{S}_\theta \simeq \kappa D_{\Gamma\Gamma} \delta\Gamma^{(1)} \sim \delta\epsilon^{-1},\tag{37}$$

where we have used the fact that $\delta\Gamma - \kappa\xi = \delta\Gamma^{(1)}$. Parameterizing the ray orbit by the enclosed magnetic flux, ψ , we look for solutions of the form $S_\theta = S_{\theta f}(\eta) + S_{\theta s}$, $\xi = \xi_f(\eta) + \xi_s$, and $S_\psi = S_{\psi f}(\eta) + S_{\psi s}$; where the subscripts f and s label the term associated with the fast and slow motion respectively. Then $\xi_f(\eta)$ satisfies

$$\begin{aligned}\frac{d\xi_f}{d\eta} \Big|_{\text{orbit}} &= \frac{d\xi_f}{dt} \Big/ \frac{d\eta}{dt} \\ &\simeq \frac{\Gamma_0 + \kappa\xi_s + \kappa\xi_f}{2\psi_0(1 + \eta/\psi_0)}\end{aligned}\tag{38}$$

This relation may be rewritten as

$$\frac{\kappa d\eta}{2\psi_0(1 + \eta/\psi_0)} = -\frac{\kappa d\xi_f}{\Gamma_0 + \kappa\xi_s + \kappa\xi_f}.\tag{39}$$

Integrating once, and using the initial data that $\xi_f = 0$ when $\eta = 0$, we obtain

$$\xi_f(\eta) = -\frac{1}{\kappa} (\Gamma_0 + \kappa\xi_s) \left[1 - (1 + \eta/\psi_0)^{-\kappa/2} \right]\tag{40}$$

or

$$\xi_f(\eta) \simeq -\Gamma_0 \frac{\eta}{2\psi_0} + \dots, \quad (41)$$

where we have used $\delta \ll 1$ in writing (41).

An analysis similar to that leading to Eq. (41) demonstrates that

$$\begin{aligned} S_{\theta f}(\eta) &= S_{\theta s} \left[(1 + \eta/\psi_0)^{\kappa/2} - 1 \right] \\ &\simeq \kappa \frac{\eta}{2\psi_0} S_{\theta s} + \dots, \end{aligned} \quad (42)$$

where we have used as an initial condition that $S_{\theta f}(\eta = 0) = 0$.

We are now ready to evaluate I_{fast} . Integrating over one cycle of the fast motion we find

$$\begin{aligned} I_{fast} &= \oint \left(S_\psi + S_\theta \frac{d\xi_f}{d\eta} \right) d\eta \\ &= \oint S_\theta \left(\frac{\Gamma}{2\psi} - \frac{\Gamma_0 + \delta\Gamma^{(0)}}{2\psi} \right) d\eta \\ &= \oint \frac{S_\theta \delta\Gamma^{(1)}}{2\psi} d\eta. \end{aligned} \quad (43)$$

Since the function $S_\theta(\eta)$ is single valued, the leading contribution to I_{fast} is

$$I_{fast} = \frac{\pi S_{\theta s}}{A} (\delta\Omega^2 + B(\xi_s)^2), \quad (44)$$

where

$$A \equiv -\frac{1}{2D_{\Omega^2}} \left[(4\psi_0^2 D_{\psi\psi} - 4\psi_0 \bar{D}_{\psi\theta} \Gamma_0 + \bar{D}_{\theta\theta} \Gamma_0^2) D_{\Gamma\Gamma} \right]^{1/2}, \quad (45)$$

and

$$B \equiv \frac{2\psi_0^2 (D_{\psi\psi} \bar{D}_{\theta\theta} - \bar{D}_{\psi\theta}^2)}{D_{\Omega^2} (4\psi_0^2 D_{\psi\psi} - 4\psi_0 \bar{D}_{\psi\theta} \Gamma_0 + \bar{D}_{\theta\theta} \Gamma_0^2)} \quad (46)$$

At this stage we have our first important result. Equation (44), together with the quantization condition $I_{fast} = \pi$, provides a quadratic equation for $S_{\theta s}(\xi_s)$,

$$H \equiv \omega \Omega_{*i} S_{\theta s}^2 - [\omega^2 + \gamma_{MHD}^2 + B\xi_s^2] S_{\theta s} + A = 0. \quad (47)$$

The solution of Eq. (47) yields the double valued function $S_{\theta s}(\xi_s)$. Our remaining quantization condition of the set (20) is simply the condition that the area enclosed by the two branches of $S_{\theta s}(\xi_s)$ in the $(S_{\theta s}, \theta_s)$ plane be equal to $(2m_s + 1)\pi$, that is

$$\oint S_{\theta s} d\xi_s = (2m_s + 1)\pi \quad (48)$$

The coefficient of S_{θ_s} in Eq. (47) is proportional to Ω_{*i} . Hence, Eq. (47) is singular in the limit $\Omega_{*i} \rightarrow 0$. The upper branch of the function $S_{\theta_s}(\xi_s) \rightarrow \infty$ as $\Omega_{*i} \rightarrow 0$. In this limit the area enclosed by the two branches of $S_{\theta_s}(\xi_s)$ is infinite if $\omega^2 < -\gamma_{MHD}^2$, and zero otherwise. Since infinity can be represented by an arbitrarily large integer, we conclude that the second quantization condition is satisfied for all frequencies $\omega^2 < -\gamma_{MHD}^2$. That is, we obtain a continuous spectrum ending at the frequency obtained from local, infinite- m analysis.

When the FLR term is included in our expression for Ω^2 [see Eq. (14)], we obtain our second important result. Equation (47) is no longer singular. Noting that our quantization condition requires $I_{fast} = (2n_f + 1)\pi$, we see that we must order $S_{\theta_s} \sim \epsilon^{-1}$ since $A \sim \epsilon^{-1}$. Similarly, we must require $\Omega_{*i} \sim \epsilon$ so that Ω^2 is of order ϵ^0 . These are crucial results since the large value of S_{θ} is necessary to justify our use of the “large m ” expansion, while the small value of Ω_{*i} indicates that ballooning modes can be stabilized even when $a_i/R_p \ll 1$. Since the splitting due to the “slow” motion is of order ϵ we may evaluate this phase integral in the local approximation, i.e

$$H = \frac{\partial}{\partial S_{\theta_s}} H = \frac{\partial}{\partial \xi_s} H = 0. \quad (49)$$

Substituting Eqs. (30) and (46) into Eqs. (49) leads to

$$\Omega_{*i} = -\frac{4\gamma_{MHD}^3}{3\sqrt{3}A} \quad (50)$$

and

$$S_{\theta} = -\frac{3A}{2\gamma_{MHD}^2} \quad (51)$$

on the marginal stability boundary. An important limitation of this model becomes apparent when we evaluate $\delta\Omega^2$. We find

$$\delta\Omega^2 = \frac{2}{3}\gamma_{MHD}^2. \quad (52)$$

Hence, this analytic model is only valid near ideal MHD marginal stability, where $\gamma_{MHD}^2 < -\delta^2|2\psi_0^2 D_{\psi\psi}/D_{\Omega^2}|$. As the system is pushed further from ideal MHD marginal stability our subsidiary expansion in δ breaks down. To some extent, this problem can be dealt with by numerically integrating ray trajectories using Eq. (31) as a model dispersion relation. Equation (31) is itself essentially a small δ expansion, so that the numerical integration of ray orbits generated from this model “Hamiltonian” also cease to give reliable results as γ_{MHD}^2 increases further. It becomes necessary to obtain the global dispersion relation by numerically integrating equations of ray motion generated from the exact (numerically determined) local dispersion relation as described in Sec. 5.

7. NUMERICAL RESULTS

Figure 8 shows the marginal stability boundary for MFTF-B in the $(\beta_c, a_i/R_p)$ plane. Stability to ideal MHD ballooning modes was not a design constraint for MFTF-B since

it was realized that ideal MHD ballooning modes would be stabilized by the kinetic effects described here. The central cell beta of MFTF-B is limited by the “rigid” ballooning mode beta limit^{17,18}, $\beta_c \leq .22$, for the values of beta in the plug cell ($\beta_p = .11$) and anchor cell ($\beta_a = .55$) assumed in these computations. The pressure in the transition region is sufficient to drive ideal MHD ballooning modes even in the absence of any central cell pressure. We have introduced an artificial negative pressure in the center cell in order to reach ideal marginal stability at $\beta_c = -0.167$. We are able to track the stability boundary from ideal MHD marginal stability at $\beta_c = -0.167$ to $\beta_c \simeq 0.1$. At this point an examination of the ray orbit shows that, while the orbit performs several rapid oscillations, it ultimately escapes like the ray orbit shown in Fig. 6. Hence, the ray orbit is no longer integrable, and the semi-classical procedure outlined in Sec. 4 is no longer justified. As long as the ray orbit continues to perform even one rapid oscillation it is possible to define I_{fast} , and to solve Eqs. (27) and (28). Points on the marginal stability boundary obtained in this manner are connected by a dashed line in Fig. 8. Figure 9 shows the values of S_θ on the marginal stability boundary. We see that the condition $S_\theta \gg 1$, required in the derivation of Eq. (1), also breaks down near $\beta_c = 0.1$. Hence, there is little significance to the dashed portion of the marginal stability curve. The effect of varying beta in the MHD anchor cell, β_a , is shown by the lower curve in Fig. 8, in which β_a has been reduced from 0.55 to 0.40. Just as in ideal MHD ballooning mode theory, we find that decreasing β_a tends to destabilize the system.

8. SUMMARY

The main result of this calculation is the marginal stability boundary shown in Fig. 8. An important feature of the marginal stability boundary is the fact that the characteristic value of S_θ , at marginal stability, decreases as β_c and Ω_{*i} increase (see Fig. 9) until the calculation breaks down at $\beta_c \simeq 0.1$. At this point $a_i/R_p = 3.3 \times 10^{-3}$, and $S_\theta = 7.27$. It is possible to extend the calculation to larger values of β_c , as indicated by the dashed curves in Figs. 8–9, but two assumptions underlying this calculation ($S_\theta \gg 1$ and integrability of the ray orbits) are not satisfied in this regime. The axicell configuration of MFTF-B lies on the right edge of Fig. 8 at $a_i/R_p \simeq 0.05$. It is clear from Figs. 8–9 that “large- m ” ballooning modes will not limit the center cell beta at these large values of a_i/R_p . The rapid decrease in S_θ on the marginal stability boundary suggests that at larger values of β_c and a_i/R_p the most dangerous modes will be low m modes with a global structure in the plane perpendicular to \mathbf{B} . The beta limit imposed by such modes is bounded from above by the “rigid” ballooning mode stability condition^{17,18} ($\beta_c < 0.22$ for these parameters). Hence, we may expect the center cell beta limit to fall in the range $0.1 < \beta < 0.22$. The extension of “large- m ” theory beyond its domain of validity gives a marginal stability boundary (the dashed curve in Fig. 8) that crosses the “rigid” ballooning mode stability limit as a_i/R_p increases. This suggests that at the rather large values of a_i/R_p in the axicell configuration of MFTF-B ($a_i/R_p \simeq 0.05$) the actual center cell beta limit will be close to the “rigid” ballooning mode stability limit of $\beta_c = 0.22$.

Acknowledgments

We gratefully acknowledge useful conversations with D.E. Baldwin, T.B. Kaiser, and

L.S. Hall. This work was performed under the auspices of the U.S. Department of Energy by the Lawrence Livermore National Laboratory under contract number W-7405-ENG-48.

REFERENCES

- ¹ J.W. Conner, R.J. Hastie, and J.B. Taylor, *Phys. Rev. Lett.* **40**, 396 (1978); A.H. Glasser, in *Proceedings of the Finite Beta Theory Workshop*, Varenna, Italy, Ed. by B. Coppi and W. Sadowski (National Technical Information Service, Springfield, 1979) p. 55.
- ² R.L. Dewar et al., *Nuclear Fusion* **21**, 493 (1981).
- ³ L.D. Pearlstein, and N.A. Krall, *Phys. Fluids* **9**, 2231 (1966).
- ⁴ M.N. Rosenbluth, N.A. Krall, and N. Rostoker, in *Proc. Plasma Phys. and Cont. Nucl. Fusion Res.*, Salzburg, 1961 (IAEA, Vienna, 1962), *Nuclear Fusion Supplement*, part 1, 143; K.V. Roberts and J.B. Taylor, *Phys. Rev. Lett.* **8**, 197 (1962).
- ⁵ K.I. Thomassen and V.N. Karpenko, "An Axicell Design for the End Plugs of MFTF-B." See National Technical Information Service Document No. 82020108 (Lawrence Livermore National Laboratory Report UCID-19318). Copies may be ordered from the National Technical Information Service, Springfield, Virginia 22161. The price is \$11.00 plus a \$3.00 handling fee. All orders must be prepaid.
- ⁶ D.E. Baldwin and B.G. Logan, "Physics Basis for an Axicell Design for the End Plugs of MFTF-B." See National Technical Information Service Document No. UCID-19359 (Lawrence Livermore National Laboratory Report UCID-19359). Copies may be ordered from the National Technical Information Service, Springfield, Virginia 22161. The price is \$14.00 plus a \$3.00 handling fee. All orders must be prepaid.
- ⁷ D.A. D'Ippolito and J.R. Myra, *Phys. Fluids* **24**, 2265 (1981).
- ⁸ see, e.g., I.C. Percival, *Adv. in Chem. Phys.* **36**, 1 (1977).
- ⁹ W.M. Tang and P.J. Catto, *Phys. Fluids* **24**, 1314 (1981); X.S. Lee and P.J. Catto, *Phys. Fluids* **24**, 2010 (1981).
- ¹⁰ W.A. Newcomb, *J. Plasma Physics* **26**, 529 (1981).
- ¹¹ L.D. Pearlstein, T.B. Kaiser, and W.A. Newcomb, *Phys. Fluids* **24**, 1326 (1981).
- ¹² D.E. Baldwin, private communication.
- ¹³ T.B. Kaiser, and L.D. Pearlstein, *Phys. Fluids* **26**, 3053 (1983).
- ¹⁴ see, e.g., B.V. Chirikov, *Phys. Reports* **52**, 263 (1979).
- ¹⁵ A.C. Hindmarsh, "Linear Multistep Methods for Ordinary Differential Equations", See National Technical Information Service Document No. UCRL-51186 (Lawrence Livermore National Laboratory Report UCRL-51186, 1972). Copies may be ordered from the National Technical Information Service, Springfield, Virginia 22161. The price is \$6.00 plus

a \$3.00 handling fee. All orders must be prepaid.

¹⁶ H. Poincaré, *New Methods in Celestial Mechanics* **3**, (1897). (Transl. NASA, Washington, D.C., 1967, document N67-27279), Chp. 27, where the theory of the surface of section is called the theory of consequents.

¹⁷ T.B. Kaiser, W.M. Nevins, and L.D Pearlstein, *Phys. Fluids* **26**, 351 (1983).

¹⁸ T.B. Kaiser and L.D. Pearlstein, *Phys. Fluids* **28**, 1003 (1985).

Figure Captions

Fig. 1. Schematic depiction of a flux surface in TMX-U. The planes $z = \pm z_T$ locate the transition regions between the central and end cells. It is in this region that flux tubes are bent by ballooning modes. The orientation of the basis vectors $\nabla\psi$, $\nabla\theta$, \hat{b} at $z = 0$ is shown along with that of the wave vector, ∇S . Also shown is the angle Υ .

Fig. 2. Critical value of β_c as a function of ψ . The values of beta in the MHD anchor cell and the axisymmetric plug cell are held fixed at $\beta_a = 0.55$ and $\beta_p = 0.11$. Theta and Γ were chosen at each value of ψ to minimize β_c .

Fig. 3. Critical value of β_c vs. Γ for $\beta_a = 0.55$, $\beta_p = 0.11$, and $\theta = 0$; ψ is held fixed at $\psi/\psi_{edge} = 0.43$.

Fig. 4. Phase-space trajectory and invariant toroid for two degrees of freedom. The C_1 and C_2 curves are for defining the action integrals I_1 and I_2 . The toroidal helix is the trajectory; normally it is not closed.

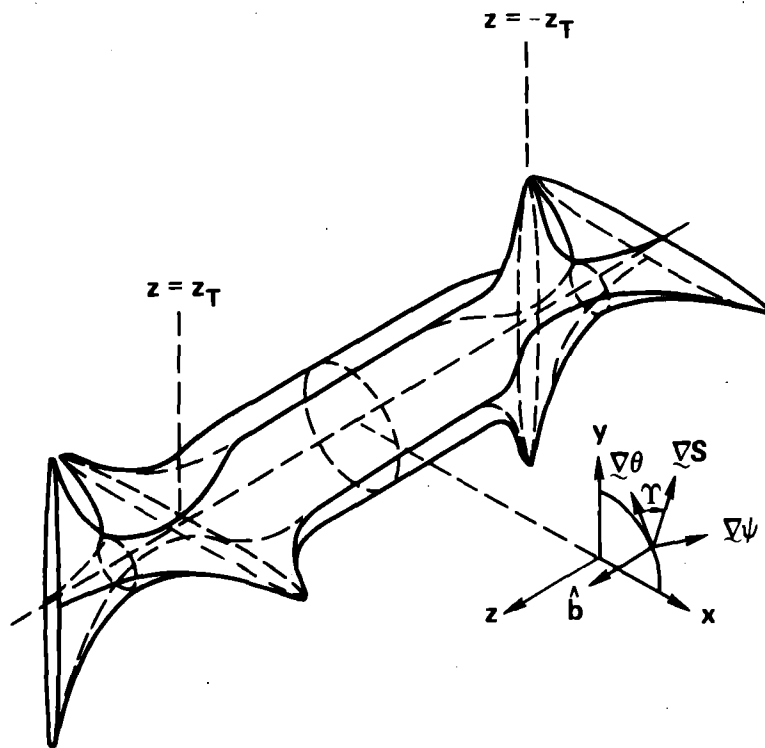
Fig. 5. An example of an integrable ballooning ray orbit: (a) the projection of the ray orbit onto the ψ , θ plane; (b) surface of section plot of S_θ vs. θ (c) points connected to form a smooth curve; and (d) our computed value of I_{fast} , which is shown to be well conserved.

Fig. 6. Same plots as in Fig. 4.2, except that the orbit is now stochastic.

Fig. 7. Sketch of the line spectrum that is characteristic of a system with well-separated time scales. Each normal-mode frequency is labeled by the WKB mode number, (n_{fast}, n_{slow}) .

Fig. 8. Marginal stability boundaries in the β_c , a_i/R_p plane. The projected operating point is $a_i/R_p \approx 5. \times 10^{-2}$. The value of β_p is 0.11, while $\beta_a = 0.55$ (upper curve) or 0.40 (lower curve). The rigid mode stability limit is $\beta_c = 0.22$ for $\beta_a = 0.55$.

Fig. 9. A plot of θ vs. β_c at marginal stability. For this plot $\beta_p = 0.11$, and $\beta_a = 0.55$.



Nevins, Pearlstein Fig. 2

